HHS Public Access

Author manuscript

Carbon N Y. Author manuscript; available in PMC 2022 June 15.

Published in final edited form as:

Carbon N Y. 2021 June 15; 177: 128–137. doi:10.1016/j.carbon.2021.02.071.

Mechanical and Viscoelastic Properties of Wrinkled Graphene Reinforced Polymer Nanocomposites — Effect of Interlayer Sliding within Graphene Sheets

Yitao Wang[1], **Zhaoxu Meng**[1]

[1]Department of Mechanical Engineering, Clemson University, Clemson, SC 29634, USA

Abstract

Multilayer graphene sheets (MLGSs) are promising nano-reinforcements that can effectively enhance the properties of polymer matrices. Despite many studies on MLGSs-reinforced polymer nanocomposites, the effect of wrinkles formed in MLGSs on the reinforcement effect and the viscoelastic properties of polymer nanocomposites has remained unknown. In this study, building upon previously developed coarse-grained models of MLGSs and poly(methyl methacrylate) coupled with molecular dynamics simulations, we have systematically investigated nanocomposites with different numbers of graphene layers and various wrinkle configurations. We find that with decreasing degree of waviness and increasing numbers of layers, the elastic modulus of the nanocomposites increases. Interestingly, we observe a sudden stress drop during shear deformation of certain wrinkled MLGSs-reinforced nanocomposites. We further conduct small amplitude oscillatory shear simulations on these nanocomposites and find that the nanocomposites with these specific wrinkle configurations also show peculiarly large loss tangents, indicating an increasing capability of energy dissipation. These behaviors are attributed to the activation of the interlayer sliding among these wrinkled MLGSs, as their interlayer shear strengths are indeed lower than flat MLGSs measured by steered molecular dynamics technique. Our study demonstrates that the viscoelastic properties and deformation mechanisms of polymer nanocomposites can be tuned through MLGS wrinkle engineering.

Graphical Abstract

Corresponding author: zmeng@clemson.edu.

Credit Author Statement

Conceptualization, Zhaoxu Meng; Data curation, Yitao Wang; Formal analysis, Yitao Wang and Zhaoxu Meng; Funding acquisition, Zhaoxu Meng; Methodology, Yitao Wang and Zhaoxu Meng; Resources, Zhaoxu Meng; Supervision, Zhaoxu Meng; Writing — original draft, Yitao Wang and Zhaoxu Meng; Writing — review & editing, Yitao Wang and Zhaoxu Meng.

Declaration of interests

The authors declare that they have no known competing financial interests or personal relationships that could have appeared to influence the work reported in this paper.

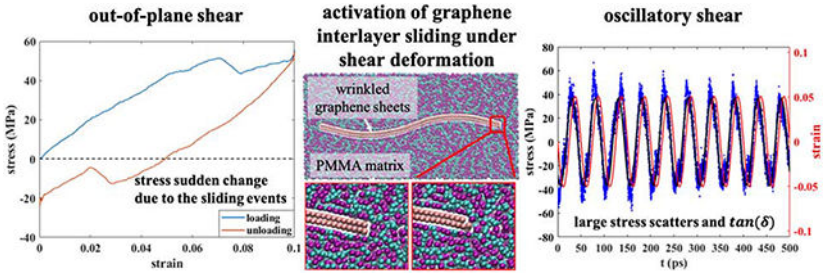

Keywords

wrinkled graphene sheets-reinforced polymer nanocomposites; coarse-grained molecular dynamics; viscoelastic properties; interlayer sliding

1. Introduction

Graphene, one-atom-thick material with sp^2 -hybridized carbon atoms and unique honeycomb lattice, has attracted considerable interest and tremendous attention from both engineering and academic communities. Graphene possesses exceptional properties such as electrical conductivity, thermal conductivity, and mechanical properties [1–3]. Graphene has been utilized in advanced applications such as electrodes of lithium-ion batteries or supercapacitors, active layers of organic solar cells, and polymer electrolyte membranes of fuel cells [4]. To leverage its remarkable mechanical properties and large surface-to-volume ratios, multilayer graphene sheets (MLGSs) have been embedded into the low modulus matrix, including polymers. Recent studies have shown that with only a small weight fraction of MLGSs, nanocomposites achieve significant enhancement in strength, toughness, and functionality [5–7]. Among all the synthesis methods, chemical vapor deposition (CVD) is arguably the most widely used method to produce MLGSs with a specific number of layers, large areas, and high quality [8].

In fact, to this date, a large number of experimental studies have demonstrated that embedding small amounts of graphene sheets can dramatically improve the mechanical properties of polymer matrices [9–11]. For instance, Wang et al. [12] produced polypropylene/graphene composites by melt compounding, spinning, and film stacking. They found that the tensile strength, tensile modulus, and interfacial strength of the composites with only 0.062 wt% graphene were improved by 117%, 116%, and 116%, respectively. The reinforcement is attributed to the high intrinsic mechanical properties of graphene platelets and the self-reinforcing mechanism. Wang et al. [13] synthesized graphene-reinforced poly(vinyl alcohol) (PVA) nanocomposites and found that the tensile strength of synthesized nanocomposites increases up to 200% with only 0.5 wt% graphene content. Similarly, Zhao et al. [14] prepared graphene/PVA composites, which achieved a 150% increase in tensile strength and an approximately 10 times increase of Young's modulus with a graphene loading of 1.8 vol%. Liang et al. [15] prepared PVA nanocomposites with graphene oxide (GO) using a simple water solution processing method. They showed a 76% increase in tensile strength and a 62% improvement of Young's modulus by the addition of only 0.7 wt% of GO due to the efficient load transfer between

the nanofiller and matrix. Naebe et al. [16] demonstrated that GO in an epoxy resin showed 22% improvement in flexural strength and 18% in storage modulus, which has been attributed to the uniform dispersion of GO and strong interfacial bonding between GO and epoxy resin.

In addition to experimental studies, computational modeling also offers significant insights into the mechanical properties and deformation mechanisms of MLGSs-reinforced polymer nanocomposites. Among different approaches, molecular dynamics (MD) simulations are among the most powerful as they can provide the ultimate details on system dynamics as well as predict the properties of systems with specific nanostructures. Most previous MD simulations are all-atomistic (AA) simulations, which include every single atom in the model. There have been extensive studies to investigate the mechanical properties of graphene sheet-reinforced nanocomposites via AA-MD simulations. For instance, Lin et al. [17] investigated the mechanical properties of graphene/ polymethyl methacrylate (PMMA) nanocomposite systems using AA-MD simulations. They showed that both the elastic and shear moduli increase with the increase of graphene volume fraction, while the efficiency of the reinforcement is reduced. Shiu et al. [18] investigated the thermal and mechanical properties of graphene/epoxy nanocomposites via AA-MD simulations. They found that the local density in the vicinity of the graphene is relatively high, and then progressively decreases to the bulk value in regions further away from the interface. The nanocomposites with intercalated graphene exhibit a higher elastic modulus, a higher glass transition temperature, and a lower thermal expansion coefficient, as the intercalated graphene can lead to larger interfacial regions. Sun et al. [19] studied the effect of functionalized graphene on the tensile properties of epoxy nanocomposites. They showed that compared with those reinforced by pristine graphene, the nanocomposites reinforced with functionalized graphene had higher elastic moduli, ultimate strength, and strain due to enhanced interfacial bonding between the functionalized graphene sheets and epoxy matrix.

A large portion of the studies considered graphene sheets as a flat sheet when conducting simulation or carrying out theoretical analysis [11, 20]. However, various reasons lead to inevitable surface corrugation within MLGSs, especially for those synthesized through CVD. Many studies have shown that thermal fluctuation [21, 22], long-range attraction forces among atoms [23], and topological defects [24, 25], all give rise to wrinkles in graphene sheets. Several studies have shown that the wrinkles of graphene can make the sheets less stiff, increase the geometrical locking effect [24], tailor the electronic structure of graphene [26], as well as influence surface properties and energy storage capability [27–30]. In addition, experimental studies have shown that graphene nanosheets exhibit highly wrinkled configurations within polymer matrices [31, 32]. There have been a few studies on the effect of nanoscale wrinkling of graphene sheet with AA-MD simulations [24, 33–36], but the system size is usually limited to tens of nanometers by focusing only on graphene sheets since AA-MD simulations are computationally expensive.

Still, the effects of wrinkles in MLGSs on the mechanical properties of polymer nanocomposites are not fully known. Moreover, how wrinkled MLGSs influence the viscoelastic properties of such nanocomposites has been minimally studied. To more effectively study the wrinkled MLGSs-reinforced nanocomposite systems, coarse-grained

(CG) models are used in this study. CG models reduce dimensionality and calculation time by grouping atoms together into beads. CG models enable us to reach larger temporal and spatial scales thereby exploring the mechanical properties of nanocomposite systems with higher computational efficiency. Our recently developed atomistically informed CG model of graphene has been shown to accurately capture mechanical properties including in-plane anisotropy, fracture behavior, and orientation-dependent interlayer shear of MLGSs while accelerating the computational speed by at least two orders of magnitude [37–40]. The CG model of polymer used in this study has also been shown to accurately capture the thermal-mechanical properties compared to atomistic simulations and experimental characterizations [41, 42]. In addition, CG-MD simulations have a unique advantage to computationally investigate the viscoelastic properties, which involve behaviors at a relatively longer period [43]. Viscoelastic properties of nanocomposites dictate the performance in many dynamic mechanical applications, such as damping [44], automotive tires [45], and impact-mitigation applications [46].

The purpose of the present work is to investigate the mechanical and viscoelastic properties of wrinkled MLGSs-reinforced polymer nanocomposite using CG-MD simulations. First, nanocomposite models of the PMMA matrix reinforced by wrinkled MLGSs with a sinusoidal wrinkle shape and different wavelengths are generated. Then, the CG-MD simulations are employed to investigate the mechanical and viscoelastic properties of the wrinkled MLGS/PMMA nanocomposites via uniaxial tensile deformation, out-of-plane shear deformation, and small amplitude oscillatory shear deformation. Furthermore, we look into specific deformation mechanisms from simulation results and provide fundamental insights into the structure-property relationships. Lastly, we will illustrate the unique effect of interlayer sliding within MLGSs on tuning the mechanical and viscoelastic properties of MLGS/PMMA nanocomposites.

2. Methods and materials

2.1. Overview of the coarse-grained models

The CG model of graphene follows a 4-to-1 mapping scheme, where four carbon atoms are represented by one CG bead. The hexagonal symmetry of the atomic lattice is conserved, which is critical to capture the interlayer shear response between graphene, including the superlubricity behavior [37, 47]. The CG force-field is developed based on a strain energy conservation approach. The CG model of PMMA employs a two-bead per monomer mapping scheme with one bead representing the backbone group and the other bead representing the sidechain methyl group. The bonded interactions, including bond, angle, and dihedral potentials, are parameterized using the inverse Boltzmann method [41, 48] to match the probability distributions from atomistic trajectories. The non-bonded interactions take the form of a 12-6 Lennard-Jones (LJ) potential and are parametrized to capture the essential thermo-mechanical properties [41]. The resulting CG models of MLGSs and PMMA are roughly 2-3 orders of magnitude more computationally efficient than the corresponding atomistic models. Illustrations of CG models of graphene and PMMA are presented in Fig. 1(a). Detailed procedures for developing the CG models can be found in the original publications [37, 41].

2.2. Nanocomposite model setup

The constructed nanocomposite model consists of wrinkled MLGSs embedded in a continuous polymer matrix, constituting a representative volume element in a typical graphene-reinforced nanocomposite. We use PMMA as the matrix material since it represents the main features of a large class of polymer materials [41]. All systems consist of PMMA chains with 100 monomers per chain, consistent with our previous studies [42]. The simulation box is set to be periodic in all three dimensions. The total length of the system (x-direction) is approximately 24 nm. The width of the system (y-direction) is about 4.2 nm. The height of the system (z-direction) is around 12.7 nm. The MLGSs have a finite length of L=20 nm, while its width is the same as that of the polymer matrix and periodic in the y-direction. The model systems enable us to focus on the effects of the waviness of MLGSs along one specific direction, the number of layers on the mechanical and viscoelastic properties of the nanocomposites, and to eliminate the size effect in the width direction. We also generate a pure PMMA system with the same number of chains to illustrate the reinforcement effect exerted by MLGSs. We note that the pure PMMA system is slightly smaller in volume than the nanocomposite systems due to the absence of MLGSs.

To represent the non-bonded interaction effectively and efficiently between graphene and polymer, LJ potential is used:

$$E_{gp} = 4\epsilon_{gp}\left[\left(\frac{\sigma_{gp}}{r}\right)^{12} - \left(\frac{\sigma_{gp}}{r}\right)^{6}\right] \quad (1)$$

where ϵ_{gp} is the depth of the potential well for the interaction between graphene beads (g) and polymer beads (p) and σ_{gp} is the distance at which the E_{gp} crosses zero. We use ϵ_{gp} = 1.2 *kcal/mol* and σ_{gp} = 4.5 Å consistently for all the models studied here. These parameter values lead to an interfacial energy of around 0.2 J m^{-2}, which is comparable to experimentally reported values between polymer matrices and graphene sheets [49]. Our future work will treat ϵ_{gp} as a tunable parameter and study its influence on mechanical properties. We note that varying ϵ_{gp} can be experimentally realized through the surface functionalization of graphene sheets as in the case of GO [43].

The initial curved surface of MLGSs is described by a sinusoidal function:

$$z = h\sin\left(\frac{2\pi x}{l}\right) \quad (2)$$

where h is the amplitude and l is the wavelength. We keep h as a constant of 1 nm. By deliberately controlling the wavelengths of wrinkles, we can generate CG graphene sheets with different configurations, i.e., waviness. The selected wavelengths include infinitely large, which corresponds to flat MLGSs, and l=40 nm, 20 nm, 10 nm, 8 nm, which give rise to 0.5, 1, 2, and 2.5 periods of sinusoidal waves, respectively. We note that in actual specimens, MLGSs exhibit more complex wrinkle configurations. The wrinkled morphology largely depends on topological defects within graphene nanosheets and specific processing conditions [25, 31, 50]. The simple while representative configurations adopted in this study

can shed light on the unique effect of wrinkles of MLGSs on mechanical and viscoelastic properties of the nanocomposites. In addition to changing the wrinkle configurations, we also alter the number of layers for MLGSs from monolayer graphene sheet to trilayer graphene sheets. Although MLGSs with more than three layers are not in the scope of this study, we believe the main conclusions in this study are transferrable to those systems. We note that the bending rigidity of MLGSs increases dramatically compared to monolayer graphene sheets [51]. As a result, highly wrinkled configurations for MLGSs with a large number of layers might be harder to achieve. A recent study also shows that the bending rigidity of multilayer van der Waals materials also depends on the interlayer shear strength [52].

2.3. Simulation procedures

To investigate the viscoelastic properties and deformation mechanisms of wrinkled MLGSs-reinforced PMMA nanocomposites, all MD simulations are carried out using the Large-scale Atomic/Molecular Massively Parallel Simulator (LAMMPS) software [53]. The results and trajectories are analyzed through the Visual Molecular Dynamics (VMD) software [54].

After generating the initial structures, we relax the structures through equilibrium simulations. First, the energy of the system is minimized using the conjugate gradient algorithm with the graphene sheets constrained in the z-direction in order to preserve the wrinkle configurations. The system is then equilibrated through thermodynamics run under an isothermal-isobaric (NPT) ensemble for 1.2 ns (the timestep is set as 4 fs). To resemble the annealing process, the temperature first rises from 300 K to 600 K in 0.2 ns, stays at 600 K for 0.2 ns, and then returns to 300 K in another 0.2 ns. The purpose of this step is to slowly and fully relax the nanocomposites to reach reasonable density and low residual stress. After the annealing process, the constraints on the graphene sheets are removed, followed by NPT equilibration for 0.4 ns at 300 K, which is to ensure the system is fully equilibrated and reaches stress and constraint-free states.

The fully equilibrated and relaxed configurations of the wrinkled bilayer graphene sheets-reinforced PMMA nanocomposites are shown in Fig. 1(b)–(f). The wrinkled structures are preserved despite tiny alterations compared to the initial configurations, and the internal stress of the nanocomposites approaches zero for all cases. The retainment of the wrinkled shape is also contributed to from the periodic nature in the other direction (y-direction). The setup of the model makes it possible to easily maintain the wrinkled shape observed for large graphene sheets due to various reasons and study the effect of wrinkled MLGSs. We note that if we did not add the z-direction constraint during the annealing process, the pre-defined wrinkle configurations would not be preserved. The aforementioned equilibration procedure is purposely designed to maintain the pre-defined wrinkle configurations. Our study also illustrates that the wrinkled features can be preserved when the polymer matrix is in the glassy state, i.e., the ambient temperature is lower than the glass transition temperature of the polymer matrix.

After the equilibration process, we carry out non-equilibrium MD (NEMD) simulations by applying deformations to the nanocomposite systems and then investigate the mechanical properties and deformation mechanisms. The different deformation schemes are also shown

in Fig. 1 (d)–(f). Uniaxial deformation is applied by drawing the unit cell along the x-direction up to the strain of ε_m with a nominal strain rate of 5×10^8 s^{-1}. During the deformation, the pressure is set as zero in y and z directions. Similarly, out-of-plane shear simulations are performed by shearing the xz-plane at a constant strain rate of 5×10^8 s^{-1}, during which the pressure in the y-direction is maintained as zero. From the simulations, we collect the stress vs. strain data for both uniaxial tension and shear deformations. Elastic moduli for both cases are obtained by fitting the slope of linear regions of stress vs. strain curves, which, in this case, is the region up to 0.02 strain.

In addition to measuring elastic moduli, we also characterized the viscoelastic behaviors of the nanocomposites through the small amplitude oscillatory shear (SAOS) approach [43]. Specifically, following the same equilibrium process, small oscillatory shear is applied on the xz-plane under the NPT ensemble at 300K. Specifically, the oscillatory shear strain ($\gamma_{xz}(t) = \gamma_0 \sin(\omega t)$) is achieved by oscillating the specified box length dimension sinusoidally as implemented in the LAMMPS code. We chose the amplitude of oscillation as 6 Å for all the systems, which leads to an oscillatory shear strain γ_0 around 0.05. We confirm that the chosen amplitude is small so that it will not lead to plastic deformation of the nanocomposite systems. The shear frequency used in this study is 2×10^{10} Hz, consistent with our previous studies [43], and is in the similar order of magnitude achieved in previous experimental studies with the quartz crystal microbalance method [55, 56]. Our previous study demonstrates that we can potentially avoid simulating over long periods and expand the understanding of viscoelastic properties under lower frequencies by measuring the dynamic moduli at elevated temperatures and applying the time-temperature superposition principle [43]. In this study, we focus on the effect of graphene wrinkle configurations on viscoelastic properties of MLGSs-reinforced nanocomposites. As a result, we only choose one representative shear frequency. The corresponding stress of the nanocomposite, which behaves viscoelastically, will exhibit a relationship with applied oscillatory shear strain as $\sigma_t = \sigma_0 \sin(\omega t + \delta)$. Then, the storage modulus G' and loss modulus G'' can be calculated as $G' = \frac{\sigma_0}{\gamma_0}\cos(\delta)$, $G'' = \frac{\sigma_0}{\gamma_0}\sin(\delta)$, and the loss tangent $\tan(\delta)$ of the nanocomposites is thus $\tan(\delta) = \frac{G''}{G'}$.

For all the NEMD simulations, we run three cycles of each with different initial configurations, and then take the average to smooth our errors and ensure the generality of the results. In addition, a total of 40 cycles are carried out in SAOS simulations. The first 30 cycles of shearing are not analyzed to eliminate potential transient effects. We fit a sinusoidal function to the stress data of the last 10 cycles and then calculate G', G'', and $\tan(\delta)$.

3. Results and discussion

3.1. Dependence of elastic modulus on wrinkle configurations and number of layers

We first compare the influence of wrinkle configurations by using the bilayer graphene sheets reinforced systems. The stress-strain curves of the bilayer graphene sheets-reinforced PMMA nanocomposites with different wavelengths under uniaxial tension are compared in

Fig. 2(a). Fig. 2(b) shows the elastic modulus measured for nanocomposites with different l and different numbers of graphene layers. In general, the elastic modulus of the nanocomposites decreases with decreasing l (i.e., increasing the waviness of the sheets). However, they all exhibit enhancements compared to the pure PMMA case. The in-plane elastic modulus of nanocomposites with wrinkled MLGSs are weakened, which is mainly attributed to the decreasing tensile stiffness of wrinkled MLGSs along the stretching direction [24]. The elastic modulus of the nanocomposites shows a sigmoidal dependence on increasing waviness of graphene sheets and it approaches the modulus of PMMA. In addition, the reinforcement effect under tension also becomes more significant with an increasing number of graphene sheets (i.e., increasing volume fraction of graphene) for flat or less wavy MLGSs. Nevertheless, when the MLGSs are highly wrinkled (i.e., l=8 nm), the enhancement in elastic modulus becomes much less dependent on the number of layers, indicating that the effect of volume fraction of MLGSs is less prominent when MLGSs are highly wavy or crumpled. This observation may guide the characterization and prediction of mechanical properties of crumpled graphene sheets based nanocomposites [57]. To examine the effect of wrinkled MLGSs on the transverse mechanical properties of nanocomposites, we also measure the elastic modulus under z-direction compression, and the results are included in Supporting Information (SI). We find that the elastic moduli of the nanocomposites also decrease with decreasing l (i.e., increasing degree of waviness), similar to the results in Fig. 2(a). This observation might be because the resistance to compression also decreases with an increasing degree of waviness.

We note that previous experimental studies have indicated that the wrinkled surfaces might be beneficial in enhancing mechanical interlocking and load transfer with the matrix [10, 31, 32]. We expect that the interfacial load transfer is influenced not only by the wrinkled configurations but also by the size of MLGSs [42, 58]. In our future work, we plan to conduct MLGSs pulling-out simulations with varying sizes of wrinkled MLGSs coupled with theoretical models to provide insight into these important questions.

3.2. Effect of interlayer sliding on out-of-plane shear deformation

This section compares the out-of-plane shear responses. Representative out-of-plane stress-strain curves up to strain of 0.1 comparing pure PMMA and nanocomposites with bilayer flat graphene sheets, wrinkled graphene sheets with different l are shown in Fig. 3(a). Shear modulus is defined as the slope of the linear regime within 0.02 shear strain. Interestingly, the reinforcement of shear modulus is not shown in the out-of-plane shear compared with the bulk polymer. This observation illustrates that the local nanoconfinement generated by graphene is less effective in shear deformation in the current case. We expect that the nanoconfinement effect on shear stiffness/modulus will become more prominent as the size of graphene sheets increases. Again, the modeling framework presented in this study coupled with theoretical analysis would be promising to bridge scales and would address these dependencies, which will be carried out in future studies.

Notably, we observe a sudden stress drop in the stress-strain curve during shear deformation of l=20 nm bilayer graphene sheet-reinforced nanocomposites. The sudden stress drop is marked with a red circle, which is an abnormal phenomenon and indicates internal

instability during shear deformation. To understand the underlying mechanism, we take a closer look into the deformation process from simulation trajectories. Fig. 3(b) shows the configurations of the nanocomposite model with bilayer graphene sheets of wavelength l=20 nm before deformation and after deformation when shear strain goes up to 0.1. We can see that there is an interlayer sliding event occurring between the graphene sheets. We further find that the occurrence of interlayer shear coincides with the sudden stress drop. We also checked the trajectories of other bilayer graphene-reinforced systems listed in Fig. 3(a), and we do not find interlayer sliding in other cases. This further confirms that the interlayer sliding is the source of the abnormal stress drop under uniaxial shear deformation.

For the l=20 nm case that shows a stress drop within the shear strain of 0.1, we further conduct the uniaxial shear deformation to a larger strain. We find that there are multiple sliding events indicated by multiple stress drops. The detailed results are included in SI. This observation indicates that the interlayer sliding within MLGSs can be continuously activated by the overall shear deformation.

We also carry out unloading simulations for the l=20 nm case, as shown in Fig. 3(c). We find that the interlayer sliding can be reversed when the global shear stress reverses direction, corresponding to the sudden stress increase below stress zero. Moreover, we run additional cycles of loading and unloading and plot them in Fig. 3(c) as well. We find that the interlayer sliding is repeatable and always reversible, and that there is a corresponding sudden stress drop and increase in the loading and unloading stress-strain curves. This observed reversible and repeatable interlayer sliding during loading/unloading cycles of shear deformation has been previously observed during nanoindentation on MLGSs [38].

We further conduct the out-of-plane shear deformation for nanocomposites with wrinkled monolayer or trilayer graphene sheets. Concerning nanocomposite systems reinforced by monolayer graphene sheets, we do not observe a stress drop for any wrinkle configurations as no interlayer sliding exists. For systems reinforced by trilayer graphene sheets, sudden stress drops and corresponding interlayer sliding are observed for both l=10 nm and l=20 nm cases, while there are no stress drops for other cases. The stress-strain curves for trilayer graphene cases are shown in the SI. We find that for the l=20 nm case, there are multiple stress drops and sliding events within the shear strain of 0.1, indicating that the interlayer shear strength within trilayer graphene of l=20 nm configuration is very low. We also include in the SI the schematics of the interlayer sliding events that happen in trilayer cases. We find that the interlayer sliding within trilayer graphene sheets, if activated, is mainly between the top layer and the bottom two layers.

This finding is non-trivial as we show that the interlayer sliding among MLGSs can be activated during the deformation of nanocomposites, despite that the graphene phase has much higher in-plane stiffness than the polymer phase. Also, the interlayer sliding seems to be activated only for MLGSs with specific wrinkled configurations. We will investigate this aspect in more detail in Section 3.4. In addition, we show that the interlayer sliding event has a direct influence on the stress response under deformation. In the next section, we further show that the interlayer sliding within MLGSs can also be activated during SAOS and affect the viscoelastic properties of nanocomposites.

3.3. Small amplitude oscillatory shear and viscoelastic properties

The oscillatory shear simulation has been widely used to study the influence of fillers on the viscoelasticity of nanocomposites [59–61]. We first focus on the bilayer graphene-reinforced PMMA system, consistent with the cases studied in the previous section. A typical stress-strain relationship of MLGS/PMMA nanocomposites shown in Fig. 4(b) is obtained from the SAOS process illustrated in Fig. 4(a). We fit the shear stress data of the last 10 cycles to a sinusoidal function. G', G'', and tan(δ) are then measured using the methods discussed in Section 2.3.

Fig. 4(c) and (d) compare the results for flat MLGSs and wrinkled MLGSs-reinforced nanocomposites (l=20 nm case). The l=20 nm case is the one that exhibits interlayer sliding of MLGS during out-of-plane shear. We can see that the l=20 nm case also shows an obvious difference in stress histories under SAOS with larger scatters and a more obvious phase lag (δ). From the SAOS simulation trajectories, we further confirm that the interlayer sliding also happens during the oscillatory shear deformation, despite that the extent of sliding is minor as the applied shear strain is small. Taken together, the results show that the interlayer sliding of MLGSs will have a significant effect on the viscoelastic properties, represented by the dynamic moduli characterized here, of MLGSs-reinforced polymer nanocomposites.

The effect of configurations of wrinkled graphene sheets on dynamic moduli (G', G'', and tan(δ)) are listed in Table 1. Our results indicate a slight decrease in G' upon the addition of MLGSs compared to pure PMMA in general. The lower G' indicates the lower capacity of the nanocomposites to store the input mechanical energy. This is consistent with our previous observation that the shear modulus is not enhanced by adding MLGSs. Although this is likely due to the small size of MLGSs used in this study, it is still necessary to enhance the interfacial adhesion between graphene and the matrix to achieve more effective reinforcement in the storage modulus. G'' and $tan(\delta)$ stand for the viscosity response of the nanocomposites. In contrast, we find that the bulk PMMA has a lower G'' and $tan(\delta)$ than that of the nanocomposites. This infers that the presence of graphene sheets may increase the internal friction loss of polymer chains or segments of the bulk PMMA, which may increase the ability to dissipate energy. These results on dynamic moduli of MLGSs-reinforced PMMA composites are consistent with our recent studies on graphene-reinforced polycarbonate systems. Generally speaking, we show that for glassy thermoplastic polymer-based nanocomposites, the addition of nanometer-scale graphene sheets does not necessarily increase G' but has a positive effect on G'', which might be related to the increased dissipation at the polymer/graphene interface.

Furthermore, the l=20 nm case shows uniquely large $tan(\delta)$ compared to other cases and bulk PMMA, consistent with the stress history comparison in Fig. 4 (c) and (d). Our results illustrate that by activating the interlayer sliding within graphene, the energy dissipation capability of the nanocomposites will be significantly enhanced, which could benefit damping or impact mitigation applications. The G' and G'' values also differ from those of nanocomposite systems without interlayer sliding within MLGSs. As a result, the interlayer sliding within MLGSs will have an impactful influence on the viscoelastic properties of the nanocomposites, which should be considered in future material characterization and design. In addition, our results also provide guidance to the dynamic mechanical analysis tests on

such nanocomposites that include MLGSs, as the interlayer sliding within MLGSs could introduce extra uncertainties to the measurement of the dynamic moduli of nanocomposites.

We also conduct SAOS simulations for wrinkled trilayer graphene-reinforced polymer nanocomposites. The dynamic modulus results are summarized in Table 2. As discussed in Section 3.2, interlayer sliding within MLGSs is observed for both l=10 nm and l=20 nm cases, while the l=20 nm case shows a larger extent of interlayer sliding. Correspondingly, these two cases also show relatively large $tan(\delta)$. In particular, the $tan(\delta)$ of l=20 nm case is approximately five times larger than the flat MLGSs-reinforced PMMA case.

3.4. Interlayer shear profile of wrinkled bilayer graphene sheets

An interesting question arises as to why the interlayer shear happens in the wavelength of l=20 nm and l=10 nm cases uniquely. To answer this question, we explore the interfacial shear strength depending on wrinkle configurations through a steered molecular dynamics (SMD) technique [37, 62–64].

To this end, we first generate free-standing bilayer graphene sheets with similar wrinkled configurations. As shown in Fig. 5(a), wrinkled bilayer graphene sheets with a wavelength of l=20 are studied using SMD to explore the interfacial shear landscape. A stiff spring is attached to the upper graphene sheet and the spring is pulled at a constant velocity of 0.1 m/s. During the pulling process, the configuration of the lower graphene sheet is constrained, and the upper graphene sheet conforms to the shape of the lower sheet, indicating the strong van der Waals force between graphene sheets restricts them from separation. The value of the spring constant (k) is critical to effectively explore the shear response. When the k value is low (i.e., the spring is soft), the force-displacement shows a non-physical stick-slip behavior (the curves are included in the SI), indicating the spring is not stiff enough to pull the upper graphene sheet with a constant velocity. Thus, such a choice of k is not able to explore the interlayer shear profile effectively. Based on different trials shown in the SI, we choose a k value of 2000 $kcal/(mol \cdot Å^2)$, which captures the realistic shear landscape with a minimal amount of noise.

We record the pulling force and scale it by the width of the graphene sheet. We then plot the scaled pulling force vs. displacement in Fig. 5(b). We neglect the initial noisy force data when the interlayer sliding is activated and shift the starting smoothed force to zero for all the curves in Fig. 5(b). Generally, the curves show a periodic response roughly associated with the periodicity of the CG graphene lattice with the scaled pulling force alternating from positive to negative values as the upper graphene sheet is pulled over interfacial energy barriers. The maximum shear force (i.e., the amplitude of the first force barrier) per unit length closely relates to the shear strength between the bilayer graphene sheets. We observe that the amplitudes of shear forces in l=20 nm and l=10 nm are relatively smaller than those of other cases. It is interesting to note that the interlayer shear strength reaches the lowest value under such wrinkle configurations. Increasing or decreasing l leads to an increase in shear strength to initiate sliding. This explains why interlayer sliding within graphene sheets is activated in the l=20 nm case. We note that the low values of shear strength for the l=10 nm case indicates the barrier for interlayer sliding is also low. The reasons why we do not observe it in l=10 nm bilayer graphene-reinforced nanocomposites might be two-fold. First,

it can be attributed to the influence of the polymer matrix. Indeed, in this simulation setup, we only consider the intrinsic shear resistance between wrinkled graphene while neglecting the influence of the polymer matrix. We anticipate that the influence of the polymer matrix might be non-negligible. Second, the wrinkled configurations of free-standing bilayer graphene are not the same as those in the nanocomposites, which have gone through extra equilibration and there are minor changes in the wrinkled configurations. These changes in configurations might also influence the interlayer shear profile.

Since we also observe the interlayer sliding in the nanocomposite with l=10 nm trilayer graphene in addition to the l=20 nm case, we further calibrate the interfacial shear profile for free-standing trilayer graphene by pulling the top layer against the bottom two layers, as this is where the main sliding events occur. The figures are included in the SI. Our results show that the l=20 nm case has minimal interlayer shear strength and the l=10 nm case has the second lowest interlayer shear strength value, whereas they are significantly lower than the other cases. These results corroborate our aforementioned findings that both l=10 nm and l=20 nm trilayer cases exhibit sliding events, while a higher magnitude of sliding happens in the l=20 nm case during uniaxial shear deformation. The results also explain the fact that $tan(\delta)$ of the l=20 nm case under oscillatory shear is significantly larger than the other cases.

We conclude that for certain wrinkled configurations of MLGSs, the interlayer shear strength can be lower than that of flat MLGSs. This interesting behavior leads to easier interlayer sliding during shear deformation of MLGSs-reinforced nanocomposites when MLGSs are moderately wrinkled. Furthermore, the interlayer sliding within MLGSs has a significant role on the viscoelastic property especially the energy dissipation capability of the MLGSs-reinforced nanocomposites. We note that a previous study reported that the interlayer shear stress increases with the extent of wrinkles [24]. However, in that study, the increasing interlayer shear stress is mainly contributed to by the vertical displacement and the rough 2D landscape. In our study, we have confirmed that there is no vertical displacement (interlayer separation) during SMD pulling without any constraints, and under this condition, the interlayer shear stress will become the lowest under certain wrinkled configurations. When MLGSs are embedded in a polymer matrix, it would become even harder for the interlayer separation to happen. Our study demonstrates that the effect of wrinkles within MLGSs is non-trivial with regard to the interfacial mechanics and viscoelastic properties of MLGSs-reinforced nanocomposites. Further studies are needed to identify additional meaningful and insightful mechanisms and to provide an optimal design of winkled MLGSs-reinforced polymer nanocomposites.

4. Conclusions

In this work, CG-MD simulations are conducted on wrinkled MLGSs-reinforced PMMA nanocomposites to investigate their mechanical and viscoelastic properties as well as detailed deformation mechanisms. We specifically focus on the effect of the waviness of wrinkled MLGSs and the number of layers on these properties. Towards this end, uniaxial tension, out-of-plane shear, and SAOS simulations are carried out on nanocomposites with different MLGS configurations.

Under uniaxial tensile deformation, we find that the addition of MLGSs into the PMMA matrix leads to an increase of elastic modulus. This reinforcement effect becomes more significant with the increasing number of graphene sheets (i.e., increasing volume fraction of graphene) and decreasing waviness. Under out-of-plane shear deformation, the enhancement of the modulus is not correlated with the addition of wrinkled graphene. We expect that the reinforcement effect under shear deformation has a strong dependence on the size of the graphene sheet, and the reinforcement effect might become significant when the graphene sheet reaches critical sizes. We will look into this size effect in more detail in our future work.

Interestingly, we observe that certain wrinkle configurations of bilayer and trilayer graphene-reinforced nanocomposites show abnormal stress drop under shear deformation, which is attributed to the activation of interlayer sliding within MLGSs. Furthermore, we carry out SAOS simulations to characterize the viscoelastic properties of nanocomposites with MLGSs of different wrinkled configurations. When the interlayer sliding within MLGSs is activated, which only happens for those specific wrinkle configurations, the nanocomposites show large $tan(\delta)$, indicating a rising level of energy dissipation. We further find that for these MLGS with specific winkled configurations, the interlayer shear strength is lower than flat MLGSs as measured by the SMD technique. Our results indicate that the interlayer sliding is more readily activated when MLGSs are moderately wrinkled, and the viscoelastic properties of the nanocomposites can be significantly altered by the interlayer sliding within MLGSs. This observation can be leveraged to design nanocomposites that more effectively dissipate the external input energy and avoid catastrophic destruction. In our future work, we will build upon our effort here to construct more realistic wrinkle configurations of MLGSs, guided by experimental observations and theoretical analysis, to understand the reinforcement effect of such MLGSs on polymer nanocomposites. We also plan to investigate the effect of number of layers of MLGSs on the corresponding wrinkle configurations and nanocomposites' physical and mechanical properties.

In conclusion, our work illustrates that the wrinkled configurations of MLGSs play a significant role in the mechanical and viscoelastic properties of MLGSs-reinforced PMMA nanocomposites. The observations and results also shed light on the interlayer shear mechanisms that give rise to these peculiar properties. More importantly, we have demonstrated that the viscoelastic properties of MLGSs-reinforced polymer nanocomposites can be tuned through wrinkle engineering of MLGSs.

Supplementary Material

Refer to Web version on PubMed Central for supplementary material.

Acknowledgments

Clemson University is acknowledged for the generous allotment of computational time on the Palmetto cluster. Z. Meng would like to acknowledge startup funds from Clemson University and SC TRIMH support (P20 GM121342).

References

[1]. Chen H, Müller MB, Gilmore KJ, Wallace GG, Li D, Mechanically strong, electrically conductive, and biocompatible graphene paper, Advanced Materials 20(18) (2008) 3557–3561.

[2]. Chen S, Wu Q, Mishra C, Kang J, Zhang H, Cho K, Cai W, Balandin AA, Ruoff RS, Thermal conductivity of isotopically modified graphene, Nature materials 11(3) (2012) 203–207. [PubMed: 22231598]

[3]. Liu Y, Xie B, Zhang Z, Zheng Q, Xu Z, Mechanical properties of graphene papers, Journal of the Mechanics and Physics of Solids 60(4) (2012) 591–605.

[4]. Sun Y, Shi G, Graphene/polymer composites for energy applications, Journal of Polymer Science Part B: Polymer Physics 51(4) (2013) 231–253.

[5]. Chandrasekaran S, Sato N, Tölle F, Mülhaupt R, Fiedler B, Schulte K, Fracture toughness and failure mechanism of graphene based epoxy composites, Composites Science and Technology 97 (2014) 90–99.

[6]. Wang J, Jin X, Li C, Wang W, Wu H, Guo S, Graphene and graphene derivatives toughening polymers: Toward high toughness and strength, Chemical Engineering Journal 370 (2019) 831–854.

[7]. Chong H, Hinder S, Taylor A, Graphene nanoplatelet-modified epoxy: effect of aspect ratio and surface functionality on mechanical properties and toughening mechanisms, Journal of materials science 51(19) (2016) 8764–8790.

[8]. Li X, Cai W, An J, Kim S, Nah J, Yang D, Piner R, Velamakanni A, Jung I, Tutuc E, Large-area synthesis of high-quality and uniform graphene films on copper foils, Science 324(5932) (2009) 1312–1314. [PubMed: 19423775]

[9]. Potts JR, Dreyer DR, Bielawski CW, Ruoff RS, Graphene-based polymer nanocomposites, Polymer 52(1) (2011) 5–25.

[10]. Rafiee MA, Rafiee J, Wang Z, Song H, Yu Z-Z, Koratkar N, Enhanced mechanical properties of nanocomposites at low graphene content, ACS Nano 3(12) (2009) 3884–3890. [PubMed: 19957928]

[11]. Montazeri A, Rafii-Tabar H, Multiscale modeling of graphene-and nanotube-based reinforced polymer nanocomposites, Physics Letters A 375(45) (2011) 4034–4040.

[12]. Wang J, Song F, Ding Y, Shao M, The incorporation of graphene to enhance mechanical properties of polypropylene self-reinforced polymer composites, Materials & Design 195 (2020) 109073.

[13]. Wang J, Wang X, Xu C, Zhang M, Shang X, Preparation of graphene/poly (vinyl alcohol) nanocomposites with enhanced mechanical properties and water resistance, Polymer International 60(5) (2011) 816–822.

[14]. Zhao X, Zhang Q, Chen D, Lu P, Enhanced mechanical properties of graphene-based poly (vinyl alcohol) composites, Macromolecules 43(5) (2010) 2357–2363.

[15]. Liang J, Huang Y, Zhang L, Wang Y, Ma Y, Guo T, Chen Y, Molecular - level dispersion of graphene into poly (vinyl alcohol) and effective reinforcement of their nanocomposites, Advanced Functional Materials 19(14) (2009) 2297–2302.

[16]. Naebe M, Wang J, Amini A, Khayyam H, Hameed N, Li LH, Chen Y, Fox B, Mechanical property and structure of covalent functionalised graphene/epoxy nanocomposites, Scientific reports 4 (2014) 4375. [PubMed: 24625497]

[17]. Lin F, Xiang Y, Shen H-S, Temperature dependent mechanical properties of graphene reinforced polymer nanocomposites—a molecular dynamics simulation, Composites Part B: Engineering 111 (2017) 261–269.

[18]. Shiu S-C, Tsai J-L, Characterizing thermal and mechanical properties of graphene/epoxy nanocomposites, Composites Part B: Engineering 56 (2014) 691–697.

[19]. Sun R, Li L, Feng C, Kitipornchai S, Yang J, Tensile property enhancement of defective graphene/epoxy nanocomposite by hydrogen functionalization, Composite Structures 224 (2019) 111079.

[20]. Awasthi AP, Lagoudas DC, Hammerand DC, Modeling of graphene—polymer interfacial mechanical behavior using molecular dynamics, Modelling and Simulation in Materials Science and Engineering 17(1) (2008) 015002.

[21]. Meyer JC, Geim AK, Katsnelson MI, Novoselov KS, Booth TJ, Roth S, The structure of suspended graphene sheets, Nature 446(7131) (2007) 60–63. [PubMed: 17330039]

[22]. Fasolino A, Los J, Katsnelson MI, Intrinsic ripples in graphene, Nature materials 6(11) (2007) 858–861. [PubMed: 17891144]

[23]. Xu R, Wang Y, Liu B, Fang D, Mechanics Interpretation on the Bending Stiffness and Wrinkled Pattern of Graphene, Journal of Applied Mechanics 80(4) (2013).

[24]. Qin H, Sun Y, Liu JZ, Liu Y, Mechanical properties of wrinkled graphene generated by topological defects, Carbon 108 (2016) 204–214.

[25]. Tripathi M, Lee F, Michail A, Anestopoulos D, McHugh JG, Ogilvie SP, Large MJ, Graf AA, Lynch PJ, Parthenios J, Papagelis K, Roy S, Saadi MASR, Rahman MM, Pugno NM, King AAK, Ajayan PM, Dalton AB, Structural Defects Modulate Electronic and Nanomechanical Properties of 2D Materials, ACS Nano (2021).

[26]. Kim E-A, Neto AC, Graphene as an electronic membrane, EPL (Europhysics Letters) 84(5) (2008) 57007.

[27]. Deng S, Berry V, Wrinkled, rippled and crumpled graphene: an overview of formation mechanism, electronic properties, and applications, Materials Today 19(4) (2016) 197–212.

[28]. Xu K, Cao P, Heath JR, Scanning tunneling microscopy characterization of the electrical properties of wrinkles in exfoliated graphene monolayers, Nano letters 9(12) (2009) 4446–4451. [PubMed: 19852488]

[29]. Zheng Q, Geng Y, Wang S, Li Z, Kim J-K, Effects of functional groups on the mechanical and wrinkling properties of graphene sheets, Carbon 48(15) (2010) 4315–4322.

[30]. Cote LJ, Kim J, Zhang Z, Sun C, Huang J, Tunable assembly of graphene oxide surfactant sheets: wrinkles, overlaps and impacts on thin film properties, Soft Matter 6(24) (2010) 6096–6101.

[31]. Ramanathan T, Abdala AA, Stankovich S, Dikin DA, Herrera-Alonso M, Piner RD, Adamson DH, Schniepp HC, Chen X, Ruoff RS, Nguyen ST, Aksay IA, Prud'Homme RK, Brinson LC, Functionalized graphene sheets for polymer nanocomposites, Nature Nanotechnology 3 (2008) 327–331.

[32]. Wan C, Chen B, Reinforcement and interphase of polymer/graphene oxide nanocomposites, Journal of Materials Chemistry 22(8) (2012) 3637–3646.

[33]. Liu F, Hu N, Ning H, Liu Y, Li Y, Wu L, Molecular dynamics simulation on interfacial mechanical properties of polymer nanocomposites with wrinkled graphene, Computational Materials Science 108 (2015) 160–167.

[34]. Shen X, Lin X, Yousefi N, Jia J, Kim J-K, Wrinkling in graphene sheets and graphene oxide papers, Carbon 66 (2014) 84–92.

[35]. Wei N, Lv C, Xu Z, Wetting of graphene oxide: A molecular dynamics study, Langmuir 30(12) (2014) 3572–3578. [PubMed: 24611723]

[36]. Wang C, Liu Y, Li L, Tan H, Anisotropic thermal conductivity of graphene wrinkles, Nanoscale 6(11) (2014) 5703–5707. [PubMed: 24781319]

[37]. Ruiz L, Xia W, Meng Z, Keten S, A coarse-grained model for the mechanical behavior of multi-layer graphene, Carbon 82 (2015) 103–115.

[38]. Wei X, Meng Z, Ruiz L, Xia W, Lee C, Kysar JW, Hone JC, Keten S, Espinosa HD, Recoverable Slippage Mechanism in Multilayer Graphene Leads to Repeatable Energy Dissipation, ACS nano 10(2) (2016) 1820–1828. [PubMed: 26783825]

[39]. Meng Z, Singh A, Qin X, Keten S, Reduced ballistic limit velocity of graphene membranes due to cone wave reflection, Extreme Mechanics Letters 15 (2017) 70–77.

[40]. Meng Z, Han J, Qin X, Zhang Y, Balogun O, Keten S, Spalling-Like Failure by Cylindrical Projectiles Deteriorates the Ballistic Performance of Multi-Layer Graphene Plates, Carbon 126 (2018)611–619.

[41]. Hsu DD, Xia W, Arturo SG, Keten S, Systematic method for thermomechanically consistent coarse-graining: a universal model for methacrylate-based polymers, Journal of chemical theory and computation 10(6) (2014) 2514–2527. [PubMed: 26580772]

[42]. Xia W, Song J, Meng Z, Shao C, Keten S, Designing multi-layer graphene-based assemblies for enhanced toughness in nacre-inspired nanocomposites, Molecular Systems Design & Engineering 1(1) (2016) 40–47.

[43]. Li T, Meng Z, Keten S, Interfacial mechanics and viscoelastic properties of patchy graphene oxide reinforced nanocomposites, Carbon 158 (2020) 303–313.

[44]. Wu J, Huang G, Qu L, Zheng J, Correlations between dynamic fragility and dynamic mechanical properties of several amorphous polymers, Journal of Non-Crystalline Solids 355(34-36) (2009) 1755–1759.

[45]. Wood CD, Chen L, Burkhart C, Putz KW, Torkelson JM, Brinson LC, Measuring interphase stiffening effects in styrene-based polymeric thin films, Polymer 75 (2015) 161–167.

[46]. Veysset D, Hsieh AJ, Kooi S, Maznev AA, Masser KA, Nelson KA, Dynamics of supersonic microparticle impact on elastomers revealed by real–time multi–frame imaging, Scientific reports 6 (2016) 25577. [PubMed: 27156501]

[47]. Feng X, Kwon S, Park JY, Salmeron M, Superlubric sliding of graphene nanoflakes on graphene, ACS nano 7(2) (2013) 1718–1724. [PubMed: 23327483]

[48]. Müller - Plathe F, Coarse - graining in polymer simulation: from the atomistic to the mesoscopic scale and back, ChemPhysChem 3(9) (2002) 754–769.

[49]. Chen X, Zheng M, Park C, Ke C, Direct measurements of the mechanical strength of carbon nanotube–poly (methyl methacrylate) interfaces, Small 9(19) (2013) 3345–3351. [PubMed: 23606544]

[50]. Ramanathan T, Stankovich S, Dikin D, Liu H, Shen H, Nguyen S, Brinson LC, Graphitic nanofillers in PMMA nanocomposites—an investigation of particle size and dispersion and their influence on nanocomposite properties, Journal of Polymer Science Part B: Polymer Physics 45(15) (2007) 2097–2112.

[51]. Gao W, Huang R, Effect of surface roughness on adhesion of graphene membranes, Journal of Physics D: Applied Physics 44(45) (2011) 452001.

[52]. Wang G, Dai Z, Xiao J, Feng S, Weng C, Liu L, Xu Z, Huang R, Zhang Z, Bending of Multilayer van der Waals Materials, Physical Review Letters 123(11) (2019).

[53]. Plimpton S, Fast parallel algorithms for short-range molecular dynamics, Journal of computational physics 117(1) (1995) 1–19.

[54]. Humphrey W, Dalke A, Schulten K, VMD: visual molecular dynamics, Journal of molecular graphics 14(1) (1996) 33–38. [PubMed: 8744570]

[55]. DeNolf GC, Sturdy LF, Shull KR, High-frequency rheological characterization of homogeneous polymer films with the quartz crystal microbalance, Langmuir 30(32) (2014) 9731–9740. [PubMed: 25019936]

[56]. Delgado DE, Sturdy LF, Burkhart CW, Shull KR, Validation of quartz crystal rheometry in the megahertz frequency regime, Journal of Polymer Science Part B: Polymer Physics 57(18) (2019) 1246–1254.

[57]. Liao Y, Li Z, Xia W, Size-Dependent Structural Behaviors of Crumpled Graphene Sheets, Carbon (2020).

[58]. Xia W, Ruiz L, Pugno NM, Keten S, Critical length scales and strain localization govern the mechanical performance of multi-layer graphene assemblies, Nanoscale 8(12) (2016) 6456–6462. [PubMed: 26935048]

[59]. Shen J, Liu J, Li H, Gao Y, Li X, Wu Y, Zhang L, Molecular dynamics simulations of the structural, mechanical and visco-elastic properties of polymer nanocomposites filled with grafted nanoparticles, Physical Chemistry Chemical Physics 17(11) (2015) 7196–7207. [PubMed: 25690511]

[60]. Raos G, Moreno M, Elli S, Computational experiments on filled rubber viscoelasticity: what is the role of particle– particle interactions?, Macromolecules 39(19) (2006) 6744–6751.

[61]. Li Z, Liu J, Zhang Z, Gao Y, Liu L, Zhang L, Yuan B, Molecular dynamics simulation of the viscoelasticity of polymer nanocomposites under oscillatory shear: effect of interfacial chemical coupling, RSC advances 8(15) (2018) 8141–8151.

[62]. Park S, Khalili-Araghi F, Tajkhorshid E, Schulten K, Free energy calculation from steered molecular dynamics simulations using Jarzynski's equality, The Journal of chemical physics 119(6) (2003) 3559–3566.

[63]. Sinko R, Keten S, Traction–separation laws and stick–slip shear phenomenon of interfaces between cellulose nanocrystals, Journal of the Mechanics and Physics of Solids 78 (2015) 526–539.

[64]. Xia W, Qin X, Zhang Y, Sinko R, Keten S, Achieving Enhanced Interfacial Adhesion and Dispersion in Cellulose Nanocomposites via Amorphous Interfaces, Macromolecules 51(24) (2018) 10304–10311.

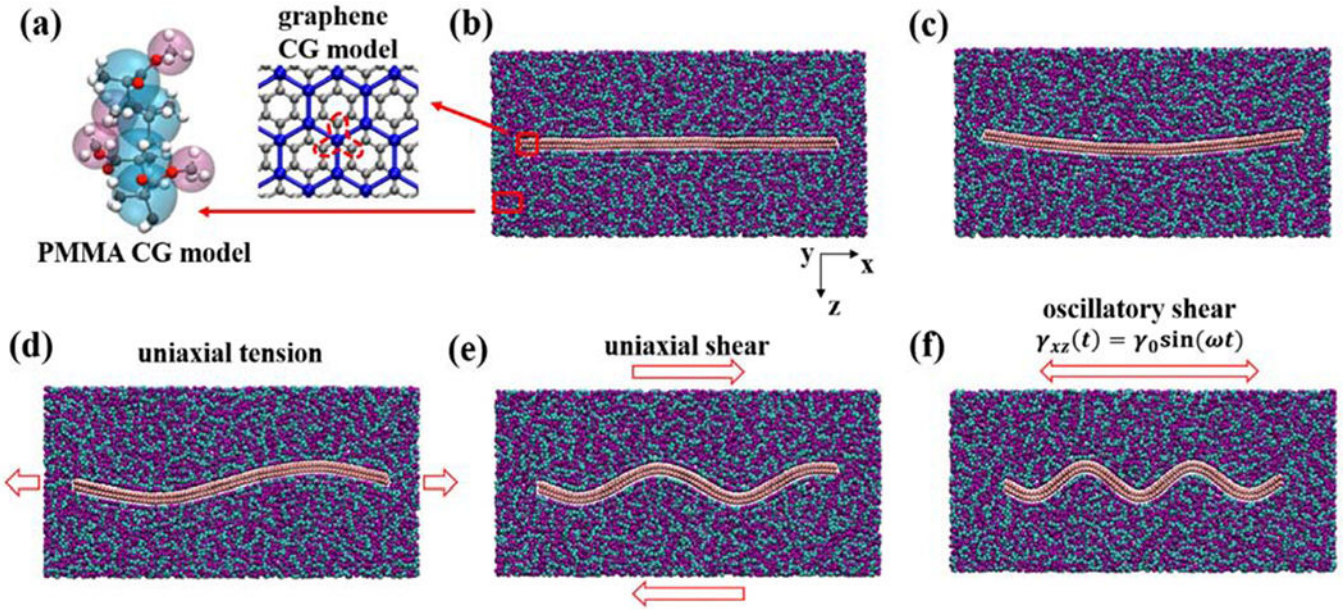

Figure 1.

Schematics of the nanocomposite models that consist of bilayer graphene sheets embedded in the PMMA matrix and mechanical tests. (a) All-atomistic (AA) to coarse-grained (CG) mapping schemes for PMMA (left) and graphene (right). The different configurations of wrinkled bilayer graphene sheets: (b) flat, (c) l=40 nm, (d) l=20 nm, (e) l=10 nm, (f) l=8 nm. The different mechanical tests carried out in this study are also shown in (d)-(f), respectively. Color code: purple and cyan for PMMA polymer beads, orange for graphene beads.

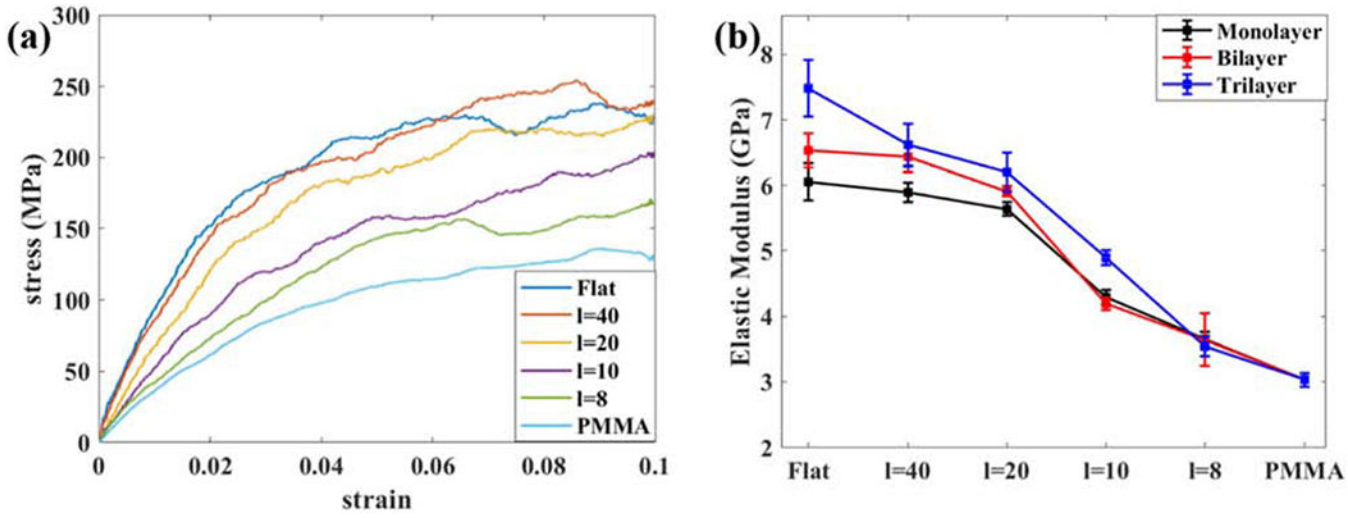

Figure 2.

Nanocomposites under uniaxial tension deformation. (a) Stress-strain curves of bulk PMMA and bilayer graphene sheets-reinforced nanocomposites with different wrinkled configurations under uniaxial tensile deformation. (b) Elastic modulus vs. different l of monolayer, bilayer, and trilayer graphene sheets-reinforced nanocomposites. The error bars show the standard deviations of results from three simulations with different initial configurations.

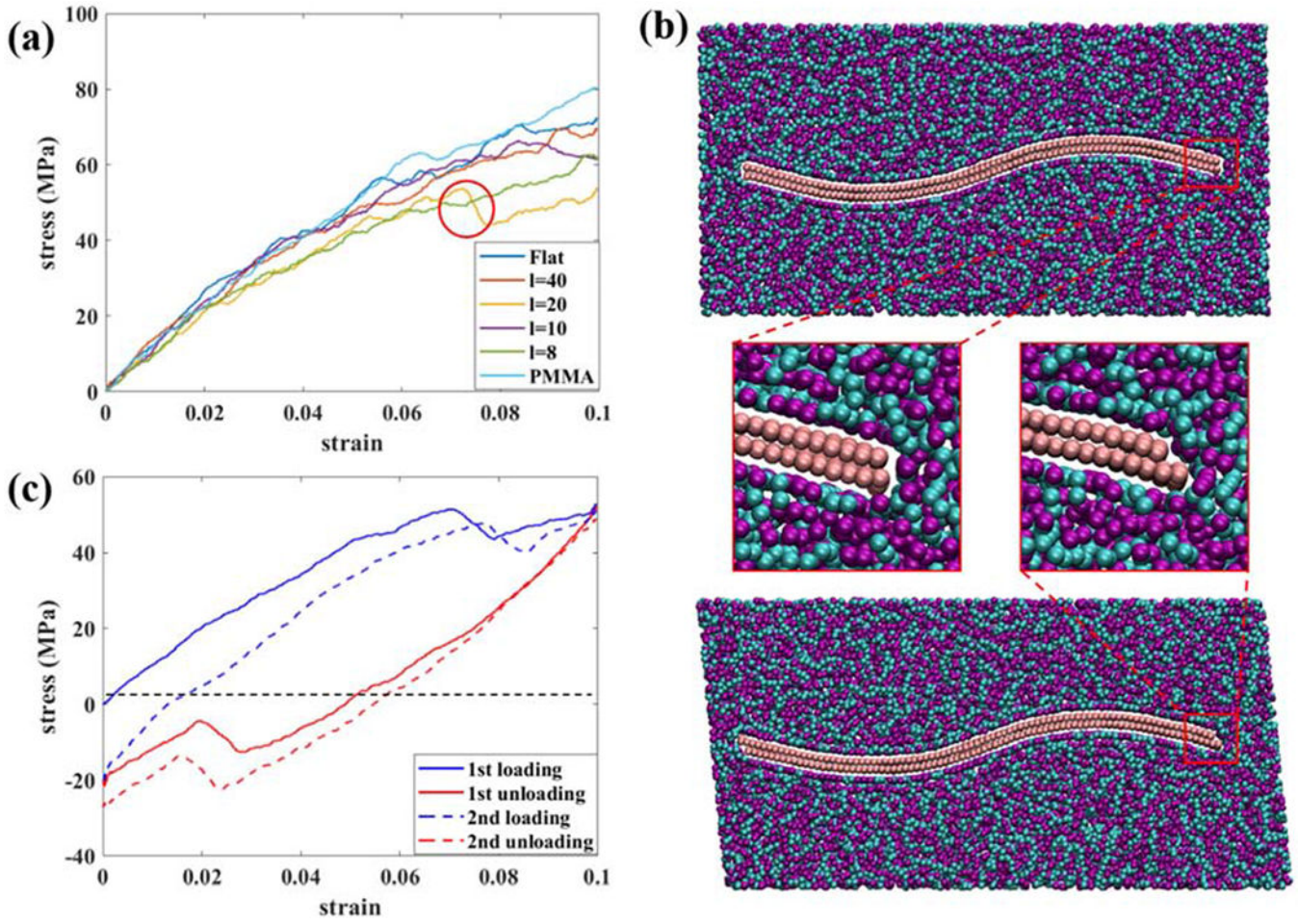

Figure 3.

The response of bilayer graphene-reinforced nanocomposites under out-of-plane shear deformation. (a) Stress-strain curves of nanocomposites with different l and pure PMMA. The sudden stress drop in the l=20 nm case is marked with a red circle. (b) Top: the nanocomposite model at a shear strain of $\gamma = 0$ (without any deformation). Bottom: the nanocomposite model at $\gamma = 0.1$. The magnified image shows the right end of the graphene sheets before and after interlayer sliding. (c) Stress-strain relationships during two loading/unloading cycles for the l=20 nm case.

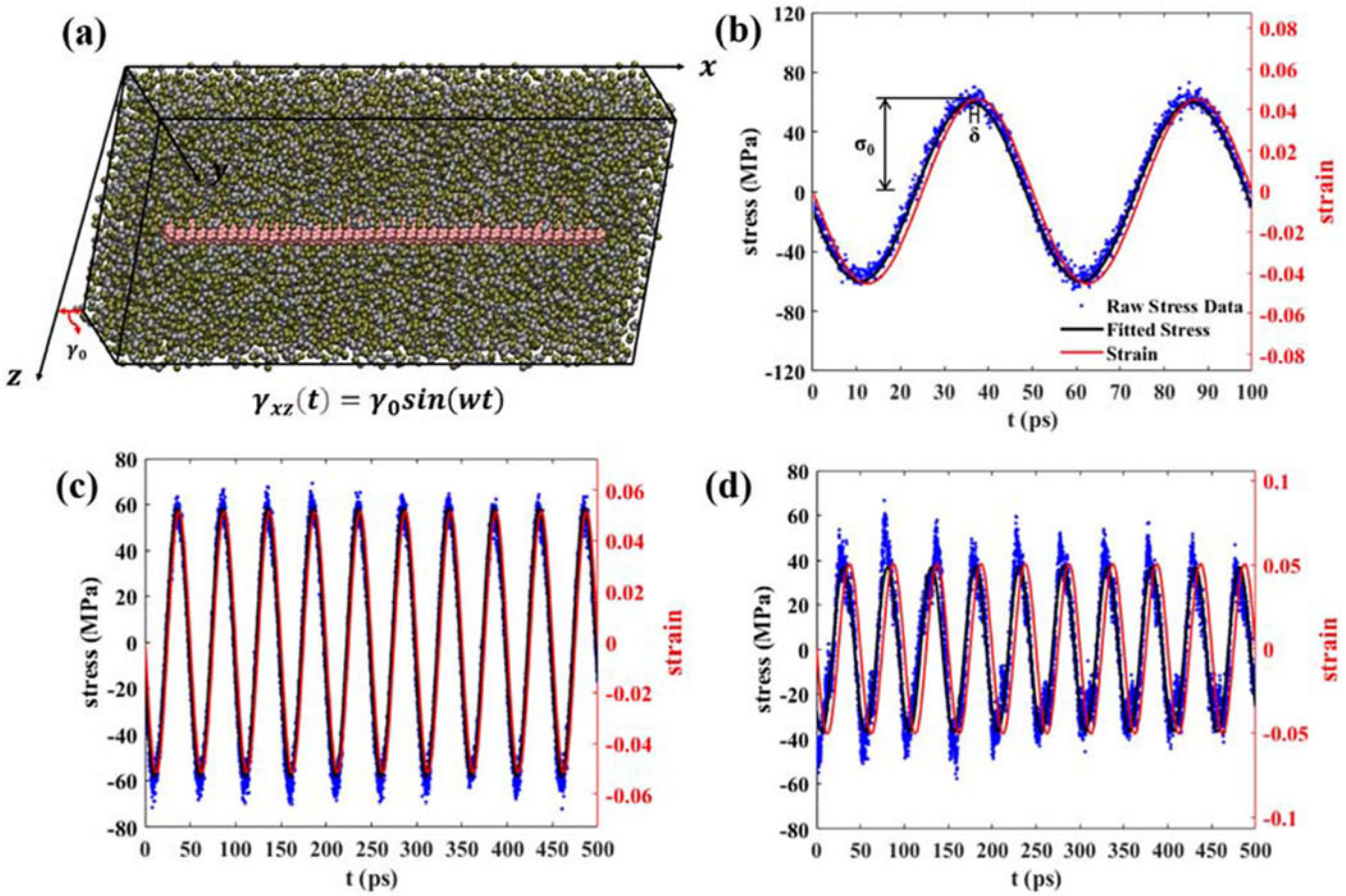

Figure 4.

SAOS simulation setup and results. (a) Oscillatory shear strain is applied in the xz-plane ($\gamma_{xz}(t) = \gamma_0 \sin(\omega t)$) and the corresponding stress is collected. (b) A typical stress-strain relationship during SAOS. The blue points indicate the raw stress data while the black and red solid lines show the smoothed shear stress and strain values, respectively. There is a phase lag δ between the stress and strain curve, which indicates the viscoelastic behavior of the system. The comparison of the last ten cycles of stress-strain relationships of nanocomposites with MLGS configurations of (c) flat and (d) L=20 nm.

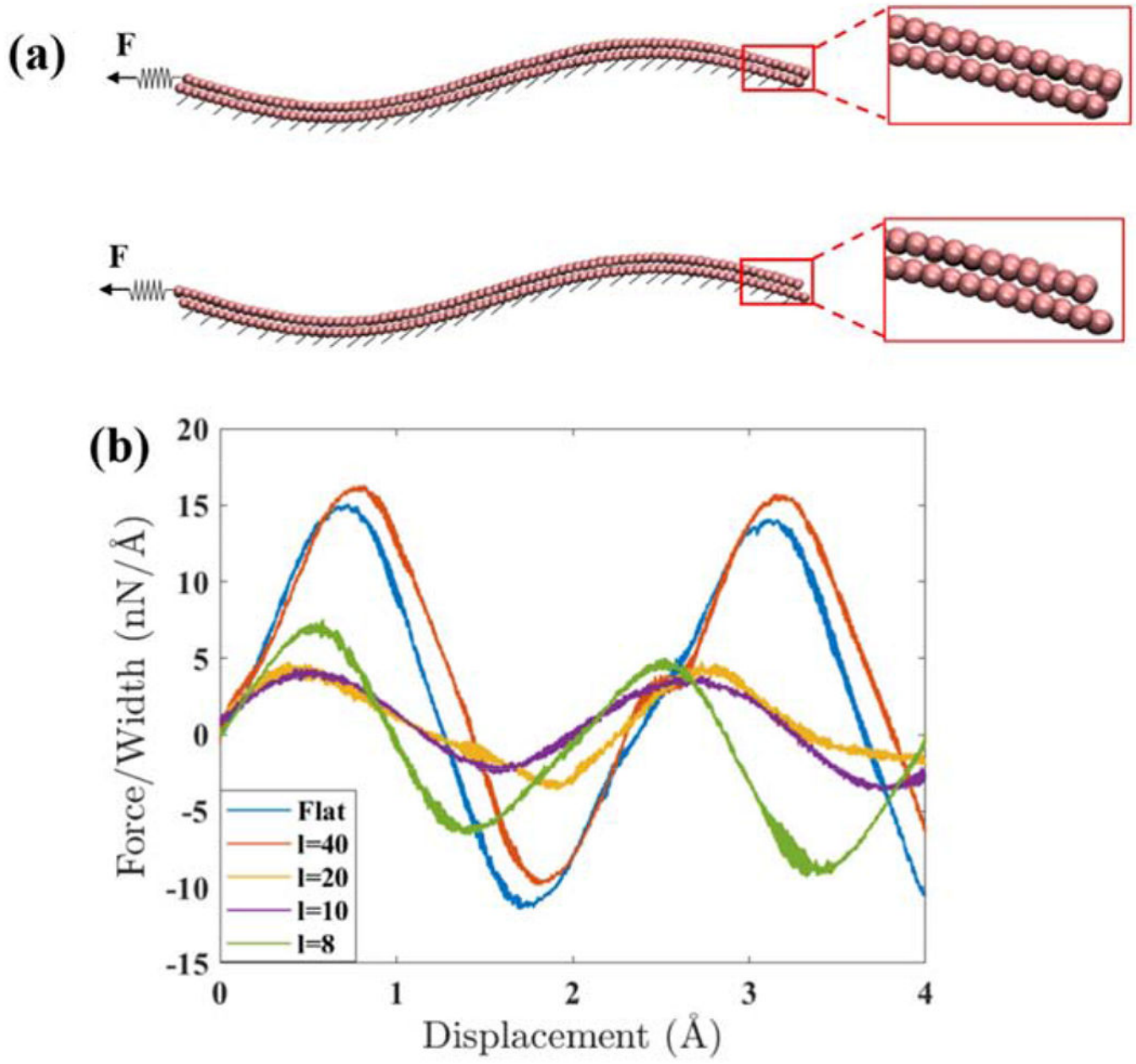

Figure 5.

Exploring the interlayer shear profile of wrinkled bilayer graphene sheets. (a) SMD simulation setup on the *l*=20 nm case, where the upper graphene sheet is pulled by a stiff spring at a constant velocity of 0.1 m/s over the bottom graphene sheet, which is constrained to its initial position. The magnified image shows the initiation of interlayer shear sliding while the graphene sheets maintaining contact in the thickness direction. (b) Comparison of the force/width vs. displacement for different configurations of bilayer graphene sheets.

Table 1.

Dynamic moduli of nanocomposites reinforced by wrinkled bilayer graphene sheets and bulk PMMA.

	Flat	***l*=40 nm**	***l*=20 nm**	***l*=10 nm**	***l*=8 nm**	**PMMA**
G'(MPa)	1097.3	1095.4	507.7	1132.7	1109.3	1311.2
G''(MPa)	303.3	305.0	523.4	294.8	308.9	236.6
$tan(\delta)$	0.276	0.279	1.031	0.260	0.279	0.181

Table 2.

Dynamic moduli of nanocomposites reinforced by wrinkled trilayer graphene sheets.

	Flat	***l*=40 nm**	***l*=20 nm**	***l*=10 nm**	***l*=8 nm**
G'(MPa)	1046.4	1101.1	335.3	1014.6	1117.7
G''(MPa)	312.9	230.8	603.4	383.8	299.3
$tan(\delta)$	0.299	0.210	1.800	0.378	0.268